Journal of Energy Storage 124 (2025) 116914

Contents lists available at ScienceDirect

Journal of Energy Storage

journal homepage: www.elsevier.com/locate/est

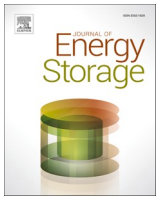

Research papers

Dynamic volumetric forces-driven phase change behavior and gradient structure design of copper foam/paraffin CPCMs

Zhaoli Zhang [a,*], Guoqin Wang [a], Nan Zhang [a], Daniela Dzhonova [b], Shady Attia [c], Yanping Yuan [a,*]

[a] School of Mechanical Engineering, Southwest Jiaotong University, Chengdu 610031, China
[b] Institute of Chemical Engineering, Bulgarian Academy of Sciences, 1113 Sofia, Bulgaria
[c] Sustainable Building Design Lab, Dept. UEE, Faculty of Applied Sciences, University of Liège, Liège 4000, Belgium

ARTICLE INFO

Keywords:
Composite phase change material
Dynamic volumetric force
Copper foam
Heat and mass transfer
Non-uniform structure

ABSTRACT

Latent heat thermal energy storage system (LHTES) based on copper foam composed phase change materials (CPCMs) has great potential in regulating the thermal management of the electronic devices. When applied in the aerospace field, heat transfer performance of CPCMs can be affected the dynamic volumetric forces, significantly impacting the temperature control of the internal electronic devices. This paper experimentally and numerically assesses the heat transfer performance of the copper foam/paraffin CPCMs under volumetric forces. The direction of the equivalent gravitational acceleration was perpendicular to the heat flux direction by adjusting the tilt angle and rotation speed of the phase change unit. Three gravity conditions, of namely microgravity, constant gravity and supergravity, are introduced in this investigation. The supergravity significantly enhances liquid natural convection, while microgravity suppresses it, thereby slowing down the melting rate of CPCMs. The porosity of the copper foam is found to be able to shorten the total melting time of CPCMs and lower the temperature of the heat wall surface. The pore density of the copper foam exerts substantial influence on the solid-liquid phase interface evolution of CPCMs. The melting time of CPCM and the heat wall temperature decrease with the augment of the pore density of the copper foam. A non-uniform gradient phase change unit consisting the high porosity copper foam in the upper part and the low porosity copper foam in the bottom part is designed to enhance the heat transfer performance. The total melting time of CPCM in the gradient phase change unit is shortened by 6.7 %, and the heat storage rate is enhanced by 7 % under normal gravity. In conclusion, the research contributes to the LHTES application subjected to various dynamic volumetric forces.

1. Introduction

The extensive application of intelligent technology has given rise to advanced and sophisticated electronic devices, which also could be considered an important evolution direction in this field [1]. The related increase in the power density of electronic devices results in the temperature rise of the devices and increasing thermal load [2,3]. Prolonged work at overheating temperature will seriously affect the stability and reliability of the electronic device operation, evolving into the main failure of the electronic equipment [4–6]. It is beneficial to develop a high-performance temperature control strategy to ensure safe and reliable operation of the electronic devices.

The LHTES technology offers the advantages of high energy storage density and nearly constant phase change temperature, making it a suitable mean to regulate the heat performance of the electronic equipment [7–9]. Moreover, the LHTES belongs to a passive temperature control without external energy input, spontaneously realizing energy storage or release based on the external temperature fluctuation. Heat transfer performance of conventional LHTES systems is restricted by the poor thermal conductivity of PCMs, leading to the inferior responsiveness to thermal loads and their applications [10,11]. The metal foam featured with stable structure, light weight and high thermal conductivity becomes a promising approach to enhance the heat transfer of PCMs [12–14].

The metal foam based CPCMs are generally prepared via the vacuum adsorption method [15–17]. Obtained results reported in available literatures demonstrate that the thermal conductivity of CPCMs can be noticeably improved by the incorporation of metal foams [18,19]. This

* Corresponding authors.
E-mail addresses: zzlyzhang@outlook.com (Z. Zhang), ypyuan@swjtu.edu.cn (Y. Yuan).

https://doi.org/10.1016/j.est.2025.116914
Received 25 December 2024; Received in revised form 21 April 2025; Accepted 1 May 2025

has the beneficial effect of accelerating the PCM phase transition rate and reducing the internal temperature gradient of PCMs [20–23]. Yang et al. [24] confirmed that the skeleton of the metal foam and the adjacent PCM exists local non-thermal equilibrium. The heat transfer performance of the CPCMs was closed related to the cell type and distribution of the metal foam. Diani et al. [25] verified that the local heat accumulation has been improved and the phase change unit containing CPCMs exhibited better temperature control performance. The porosity of the metal foam is found to have negative effect on phase change heat transfer of CPCMs. The lower porosity of the metal foam leads to a faster melting rate of the CPCMs. Meng et al. [26] ascertained that the total melting time was reduced by 68.7 % when the porosity reduced from 98 % to 88 %. Contrarily, the heat transfer performance of the CPCMs can only be slightly affected by the pore density of the metal foam. Whereas, addition of the metal foam will decrease the volume of PCMs and inhibit the flow of liquid PCMs.

The pore distribution of metal foam also significantly impacts the phase change heat transfer characteristics of CPCMs [27]. Joshi et al. [28] designed the phase change unit filled with the 75 % metal foam to make full use of the liquid natural convection, basically achieving the identical effect to the metal foam fully filled case. Shen et al. [29] found that a graded pore density structure effectively improved temperature uniformity in the early stages of melting, with the combination of 30 PPI and 40 PPI reducing temperature differences along the same horizontal plane by 71.4 %. Guo et al. [30] discovered that a smaller difference between the inside and outside subregions resulted in more intense natural convection and better thermal performance. The optimally adaptive metal foam strategy could significantly shorten the melting duration up to 17.15 %. Li et al. [31] proposed a nonuniform structure for the composite PCM to address the solid PCM dead zone when applied in PV thermal management. The energy density of a case with a dead zone porosity of 0.80 was 6.8 % higher than that with a dead zone porosity of 0.95. Kotb et al. [32] suggested that positive porosity gradients significantly improved the melting rate and energy storage performance. It is specifical that a positive gradient in the x-direction and y-direction reduced the melting time by 10.4 % and 16.74 % compared to the uniform porosity configuration. In all, the above researches indicate that PCMs incorporated into the non-uniform structure of metal foam present excellent flow characteristic, leading to noticeable improvements in local heat transfer within the CPCM region. An enhancement in overall heat transfer performance of the CPCMs can be rationally achieved in the no-uniform strategy.

Phase change thermal management systems for aircrafts, power cars and other electronic devices will be subjected to dynamic forces other than gravity due to changes in acceleration and deceleration environment [33,34]. The dynamic volume force will play a substantial role in heat transfer and liquid flow of the PCMs, complicating the phase change heat transfer of metal foam based CPCMs. Numerous studies have employed an article image velocimetry (PIV) technology to measure the phase transition interface and velocity of PCM within the phase change units installed in a rotating visualization experimental device [35–38]. Changing the centrifugal force can generate various equivalent gravitational forces. Li et al. [39] identified that the natural convection of PCM played a key role in the melting process. The heat transfer mechanism of CPCMs changed from convection-dominated to heat conduction-dominated with the augment of supergravity. Kansara et al. [40] found that microgravity had significant influence on melting of CPCMs while less impact on their solidification. The PCM average liquid fraction gradually decreased by 18 % as the value of gravitational acceleration reduced from g to g/80. Li et al. [41] disclosed that increasing the supergravity made the CPCM melting interfaces more inclined, which resulted from the interaction of primary convection and secondary convection during the charging process. Other studies showed that heat transfer performance of CPCMs hardly changed with the pore density variation of the metal foam [42,43,45,46]. Wang et al. [44] discussed the effect of heat source location on the melting behavior of CPCMs under supergravity. The bottom heating was found to be the optimal location, saving approximately 60.24 % melting time compared to the side heating case.

These previous finds suggest that the utilization of metal foam represents an effective methodology to improve the low thermal conductivity of PCM. The configuration of the metal foam facilities thermal storage enhancement of the phase change units. The change in external force can significantly alter the natural convection of liquid PCM, which in turn affects the temperature distribution and phase interface development of CPCMs inside the thermal storage units. However, there is limited research towards the shift between thermal conduction and convection of PCMs in response to gravitational forces. Temperature of the heat source and the temperature distribution of the PCM inside the phase change units subjected to supergravity and microgravity have been largely unexplored. Only limited attentions have been paid to the detailed layout of the metal foam to address the heat transfer performance of the phase change units. This paper aims to investigate the phase change heat transfer of CPCMs during the melting process under various dynamic force conditions. A two-dimensional numerical model of the phase change units is established based on the experiments. Effect of the pore parameter on heat transfer of CPCMs in response to diverse gravitational forces is then numerically evaluated. A gradient metal foam strategy is finally developed with the objective of optimizing the CPCM heat transfer performance. The expected research findings will contribute to reveal influence of the dynamic load on the heat transfer mechanism of CPCM.

2. Methodology

A combination of experimental testing and numerical simulation are employed in this investigation. The numerical model is firstly built on the basis of a rational physical model. The experimental results are then conducted to determine the phase change heat transfer characteristics. Obtained experimental results are further utilized to verify the numerical model. This paper adopts the validated numerical model to analyze the impact of pore parameters in the copper foams on heat transfer performance of the CPCMs subjected to various gravitational forces.

2.1. Experimental test

This paper employs a mechanically rotating platform to conduct equivalent experiments, as illustrated in Fig. 1. The experimental apparatus consists of five modules: a phase change unit, a DC power, a data acquisition instrument and a computer. The power module mainly includes a motor, a turntable, a base and a speed controller. The turntable is driven by a motor through a shaft, and its speed is adjusted by a speed regulator with the purpose of simulating an equivalent dynamic volume force. The phase change units are composed of paraffin, copper foam, a PC container and a thermal insulation shell. The copper foam (80 mm × 80 mm × 10 mm, Kunshan GuangJiaYuan new materials *Co.* Ltd., China) is first positioned within the PC container. The paraffin RT42 is used as the PCM with the thermophysical properties listed in Table 1 [35,36]. The liquid paraffin pre-melted at 338.15 K is then injected into the PC container in a stepwise manner to prevent the formation of bubbles. The phase change units generally solidify at room temperature and the excess paraffin is polished. The upper surfaces of the phase change units are sealed with the aid of sealants. Several thermal couples are buried into the phase change units to accurately record the transient temperatures of the phase change unit. The phase transition interface is captured at five-minute intervals using a digital camera.

The supergravity/microgravity simulated in this study are represented by an equivalent static volumetric force. This method is valid for investigating effects of steady forces on phase change heat transfer. The phase change unit is subjected to two working forces of gravity and centrifugal force. The direction of the combined force is in parallel with

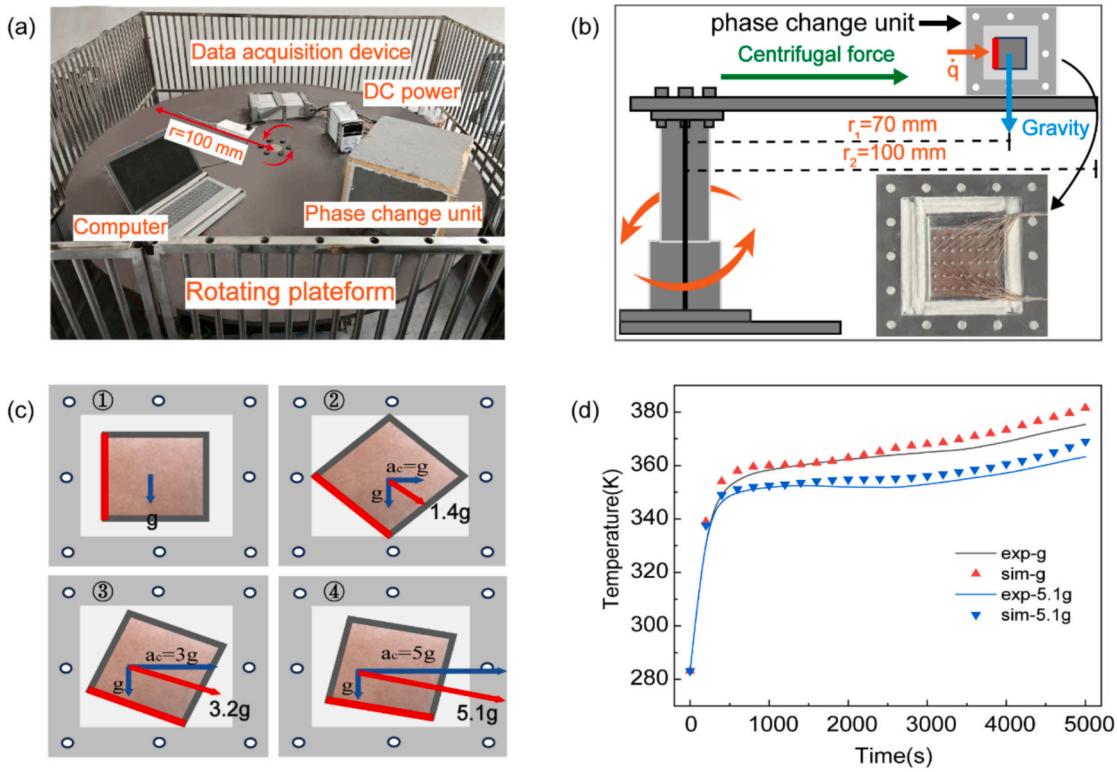

Fig. 1. Model verification analysis, (a) Experimental set-up; (b) Experimental principle; (c) Equivalent supergravity and (d) Comparison between experiment and simulation.

Table 1
Thermophysical properties of PCMs.

Thermophysical properties	Values
Density (solid/liquid)	920/880 kg/m^3
Specific heat (solid/liquid)	2200/1800 J/(kg·K)
Conductivity (solid/liquid)	0.22/0.18 W/(m·K)
Dynamic viscosity	0.003 Pa·s
Latent heat	197,700 J/kg
Thermal expansion coefficient	0.00111 /K
Solid temperature	314.15 K
Liquid temperature	320.15 K

the heating wall, through simultaneously regulation of the tilt of the phase change unit and the magnitude of the centrifugal force. The direction of the heat flow is always maintained perpendicular to that of the combined working force during the experimental test. The lateral heating of devices under various gravitational forces is implemented during the experiments. The actual gravity is a vector synthesis of the horizontal centrifugal force and vertical gravity through Eq. (1). Taking the experimental conditions and safety into consideration, this paper selects four centrifugal forces of 0 *g*, 1 *g*, 3 g and 5 g. The corresponding supergravity is determined as 1 g, 1.4 g, 3.2 g and 5.1 g with the angles between the phase change unit and the horizontal direction of 90°, 45°, 18.4° and 11.3°, respectively.

$$a_h = \sqrt{(\omega^2 r)^2 + g^2} \tag{1}$$

where a_h is the supergravity, m/s^2; ω is the rotating angular velocity of the phase change unit, rad/s; r is the rotating radius of the thermal energy storage unit, m; g is the constant gravity, g = 9.81 m/s^2.

The detailed experiments are conducted as follows: The whole experimental system is firstly suffered to a centrifugal force to create a target external force environment. The heating module is then turned on when the experimental system reaches a stable state. The thermal performance of PCMs will be measured in the next step. We adopt the reverse order to shut down the devices when the experimental determination is finished. Given that the time to reach heating stability is relatively short, it is rational to neglect its impact on the experimental findings. We also have added this part into the manuscript.

The accuracy and method of measurements is calculated in this investigation. The distance between the heat storage unit and the center of the circle is about 1.2 %. The uncertainty of the rotational speed is 1.7 %. Therefore, the uncertainty of the centrifugal acceleration is 2 %. The temperature uncertainty based on the K-type thermocouples is 1 %. Through theoretical calculations and actual weighing, it was found that the mass error of CPCM is about 2.8 %. The uncertainty of PCM complete melting time is about 1.6 %. The uncertainty of the true density of the heat flux absorbed by the thermal storage unit is about 4.8 %. The uncertainty of latent heat storage rate is 3.2 %.

2.2. Numerical simulation

2.2.1. Governing equations

A two-dimensional physical model of CPCMs embedded in the phase change unit is built in this paper as illustrated in.

Fig. 2 A two-dimensional physical model of CPCMs.

(1) The natural convection of liquid due to the thermal buoyancy is subjected to the Boussinesq assumption;
(2) The liquid PCM inside the phase change unit is incompressible and its flow state is termed as unsteady laminar flow;
(3) The copper foam is an isotropic uniform material and the flow of liquid PCM embedded in the copper foam conforms to the Darcy law;
(4) Thermophysical parameters of the copper foam and PCM are constant during the melting process.

Based on the above assumption, the detailed governing equations in

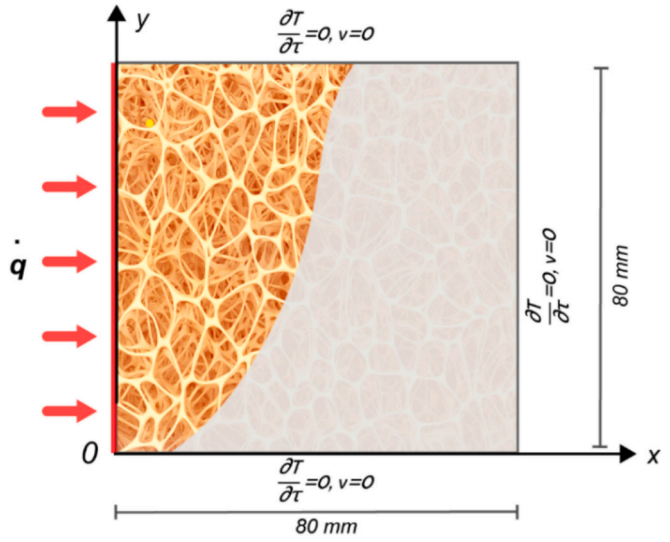

Fig. 2. The enthalpy-porosity method is utilized to solve the phase change heat transfer of PCMs and the following assumptions are made prior to the numerical simulation.

terms of continuity equation, momentum and energy conservation equation are listed as follows:

(1) Continuity equation

$$\left(\frac{\partial(\rho_{pcm}u)}{\partial x}\right)+\left(\frac{\partial(\rho_{pcm}v)}{\partial y}\right)=0 \tag{2}$$

(2) Momentum conservation equation

$$\frac{1}{\varepsilon}\left(\frac{\partial(\rho_{pcm}u)}{\partial t}\right)+\frac{1}{\varepsilon}\left(\frac{\partial(\rho_{pcm}uu)}{\partial x}+\frac{\partial(\rho_{pcm}vu)}{\partial y}\right)=-\frac{\partial p}{\partial x}+\frac{\mu}{\varepsilon}\left(\frac{\partial^2 u}{\partial x^2}+\frac{\partial^2 u}{\partial y^2}\right)+S_x \tag{3}$$

$$\frac{1}{\varepsilon}\left(\frac{\partial(\rho_{pcm}v)}{\partial t}\right)+\frac{1}{\varepsilon^2}\left(\frac{\partial(\rho_{pcm}uv)}{\partial x}+\frac{\partial(\rho_{pcm}vv)}{\partial y}\right)=-\frac{\partial p}{\partial y}+\frac{\mu}{\varepsilon}\left(\frac{\partial^2 v}{\partial x^2}+\frac{\partial^2 v}{\partial y^2}\right)+S_y \tag{4}$$

$$S_x=A_{mush}\left(\frac{(1-f)^2}{f^3+\eta}\right)u-\frac{\mu}{K}u-\frac{1}{\sqrt{K}}C_i\rho_{pcm}u\sqrt{u^2+v^2} \tag{5}$$

$$S_y=A_{mush}\left(\frac{(1-f)^2}{f^3+\eta}\right)v-\frac{\mu}{K}v-\frac{1}{\sqrt{K}}C_i\rho_{pcm}v\sqrt{u^2+v^2}+\rho_{pcm}a\beta(T-T_m) \tag{6}$$

where S_x and S_y are the resistance source terms in x, y directions, respectively; ρ is the density of material, kg/m^3; u, v is the velocity in x, y directions, m/s; τ is the time, s; ε is the porosity of copper foam; μ is the dynamic viscosity, Pa·s; A_{mush} is the coefficient of mushy area; η is the constant; C_i and K denote the inertia resistance coefficient and the permeability; β refers to the thermal expansion coefficient; α represents the acceleration in the direction of gravity.

The mushy zone constant A_{mush} and liquid fraction threshold η are set to 1×10^5 and 0.001 [38], respectively, following the recommendations of Brent [39] and Voller [40]. These values ensure negligible artificial damping in the liquid region ($f \to 1$) while suppressing unphysical velocities in the solid region ($f \to 0$).

(3) Energy conservation equation

Since there exists thermal non-equilibrium between copper foam and PCMs, two energy conservation equations are built in this investigation.

For PCM:

$$\varepsilon\left(\frac{\partial(\rho c_p T_p)}{\partial \tau}\right)+\varepsilon\left(\frac{\partial(\rho c_{pcm}u)}{\partial x}+\frac{\partial(\rho c_{pcm}v)}{\partial y}\right)=\frac{\partial}{\partial x}\left(k_{e,pcm}\frac{\partial T_{pcm}}{\partial x}\right)$$
$$+\frac{\partial}{\partial y}\left(k_{e,pcm}\frac{\partial T_{pcm}}{\partial y}\right)-\varepsilon\rho L_h\frac{\partial f}{\partial \tau}+h_{sf}\alpha_{sf}(T_s-T_{pcm}) \tag{7}$$

For copper foam:

$$(1-\varepsilon)\left(\frac{\partial(\rho c_{cu}T_{cu})}{\partial \tau}\right)=\frac{\partial}{\partial x}\left(k_{e,cu}\frac{\partial T_{cu}}{\partial x}\right)+\frac{\partial}{\partial y}\left(k_{e,cu}\frac{\partial T_{cu}}{\partial y}\right)+h_{sf}a_{sf}(T_{pcm}-T_{cu}) \tag{8}$$

where k_e, $k_{e,pcm}$ and $k_{e,cu}$ are the effective thermal conductivity of CPCM, PCM and copper foam, respectively, W/(m·K); c is specific heat capacity of PCM, J/(kg·K); L is latent heat of PCM, J/kg; h_{sf} is the interfacial heat transfer coefficient between PCM and copper foam, W/(m^2·K); α_{sf} is the surface area of the copper foam skeleton, m^2; f is the liquid fraction obtained from Eq. (9).

$$f=\begin{cases}0 & , \quad T<T_{m1}\\ \dfrac{T-T_{m1}}{T_{m2}-T_{m1}} & , \quad T_{m1}<T<T_{m2}\\ 1 & , \quad T>T_{m2}\end{cases} \tag{9}$$

where T is transient temperature of PCM, K; T_{m1} and T_{m2} are respectively the solidification and melting temperatures of PCM, K.

2.2.2. Thermophysical properties of copper foam

Structurally speaking, the copper foam consisting of a metal skeleton structure and the internal interstitial spaces is assumed to have homogeneous porosity and isotropic pore distribution. It can be characterized by parameters such as pore diameter (d_p), skeleton diameter (d_l) and specific area (α_{sf}). These parameters are determined through the following empirical Eqs. (10)–(12).

$$d_p=0.0254/PPI \tag{10}$$

$$d_l=1.18\cdot d_p\cdot\sqrt{\frac{1-\varepsilon}{3\pi}}\Big/\left(1-e^{-\frac{1-\varepsilon}{0.04}}\right) \tag{11}$$

$$a_{sf}=3\pi\frac{\left(1-e^{-\frac{1-\varepsilon}{0.04}}\right)}{(0.59d_p)^2}d_l \tag{12}$$

where PPI and ε are pore density and porosity of the copper foam.

The viscous resistance and inertial resistance experienced by PCM flowing inside the copper foam is described through the empirical equations established by Mahajan [41]. Relations of the permeability (K) and inertial resistance coefficient (C_i) are exhibited in Eqs. (13)–(14).

$$K=0.00073(1-\varepsilon)^{-0.224}\left(\frac{d_l}{d_p}\right)^{-1.11}{d_p}^2 \tag{13}$$

$$C_i=0.00212(1-\varepsilon)^{-0.132}\left(\frac{d_l}{d_p}\right)^{-1.63} \tag{14}$$

The interfacial heat transfer coefficient (h_{sf}) between the copper foam and PCM is calculated by means of the empirical Eq. (15).

$$h_{sf} = \begin{cases} \dfrac{0.76Re_p^{0.4}Pr^{0.37}k_p}{d_l} & , \quad 0 < Re_p < 40 \\ \dfrac{0.52Re_p^{0.5}Pr^{0.37}k_p}{d_l} & , \quad 40 < Re_p < 1000 \\ \dfrac{0.26Re_p^{0.6}Pr^{0.37}k_p}{d_l} & , \quad Re_p > 1000 \end{cases} \tag{15}$$

where Re denotes Reynolds number, $Re_p = \rho d_l \vec{u}/\mu\varepsilon$; Pr represents Prandtl number, $Pr = c_\rho \mu/\lambda$.

The widely accepted empirical equation proposed by Boomsma is employed in this study to calculate equivalent thermal conductivity (k_{eff}) of the copper foam [42].

$$k_{eff} = \frac{1}{\sqrt{2}(M_A + M_B + M_C + M_D)} \tag{16}$$

$$M_A = \frac{4\sigma}{(2e^2 + \pi\sigma(1-e))k_c + (4 - 2e^2 - \pi\sigma(1-e))k_p} \tag{17}$$

$$M_B = \frac{(e-2\sigma)^2}{(e-2\sigma)e^2k_c + (2e - 4\sigma - (e-2\sigma)e^2)k_p} \tag{18}$$

$$M_C = \frac{\left(\sqrt{2} - 2e\right)^2}{2\pi\sigma^2(1-2\sqrt{2}e)k_c + 2\left(\sqrt{2} - 2e - \pi\sigma^2(1-2\sqrt{2}e)\right)k_p} \tag{19}$$

$$M_D = \frac{2e}{e^2k_c + (4-e^2)k_p} \tag{20}$$

$$\sigma = \sqrt{\frac{\sqrt{2}(2 - 5/8e^3\sqrt{2} - 2\varepsilon)}{\pi(3 - 4e\sqrt{2} - e)}}, e = 0.339 \tag{21}$$

2.3. Model solving

2.3.1. Boundary and initial conditions

The left surface of the phase change unit is assumed as a heat flux boundary of 5200 W/m^2 in the temperature field, while the other surfaces are defined as thermal insulation boundary. The initial temperature of the whole phase change unit is set as 297 K. Given that the liquid PCM will flow within the studied region under the drive of the thermal buoyancy, the flow field is coupled with the temperature field. The surfaces of the phase change unit are designed as no-slip boundary with the corresponding velocity of 0 m/s.

2.3.2. Solving method

Phase change heat transfer of CPCM is studied through the finite volume method built in the commercial Fluent 2021R1. The PISO is applied to the pressure-velocity coupling, while a first-order implicit scheme is utilized to discretize the non-stationary term. The pressure is corrected through the PRESTO! algorithm. The momentum and energy conservation equations are discretized through a second-order windward scheme. The relaxation factors of pressure, velocity, energy and liquid fraction are set individually to 0.3 , 0.7, 0.9 and 1. The convergence criteria of continuity, momentum and energy conservation equations are 10^{-6}, 10^{-4} and 10^{-4}, respectively.

2.3.3. Model independence

The efficiency and accuracy of numerical investigation are closely related to the mesh quantity and the time step. Therefore, it necessitates to carry out their independence verification. This paper compares fractions of liquid PCMs under three grid numbers (20,000, 40,000 and 80,000) and three iteration time steps (0.01 s, 0.1 s and 0.5 s). Fig. 3 indicates that discrepancies in the calculated results are separately <0.50 % and 0.42 % when the mesh number and time step are larger than 40,000 and 0.1 s. Furthermore, in order to·guarantee·the accuracy and efficiency of the numerical study, the grid number of 40,000 and the iteration time step of 0.1 s are employed in the calculation.

2.4. Model verification

The reliability of the numerical model is evaluated through the comparison between the simulation results and the experimental results obtained under the identical boundary conditions. The simulation calculation results are compared with the experimental results in terms of temperature for PCM situated at the center of the phase change unit. Fig. 1(d) indicates that the simulation results are highly consistent with experimental results. The boundary conditions except for the heat source are hypothesized as adiabatic in the simulation calculation, resulting in the PCM temperature rising slightly faster than the experimental values. The deviation between the simulated temperature and the measured temperature is calculated to be no >3.9 %. It is obtained that the numerical model and calculation method adopted in this paper are suitable for the reliable investigation of phase transition in phase change units.

3. Results and discussion

3.1. Gravity magnitude

Fig. 4 illustrates phase contours and temperature profiles of CPCM under various supergravity. It is observed that the phase change heat transfer at the initial stage ($t \leq 900$ s) is dominated by conduction, when the supergravity is limited (a = g and a = 1.4 g). The temperature

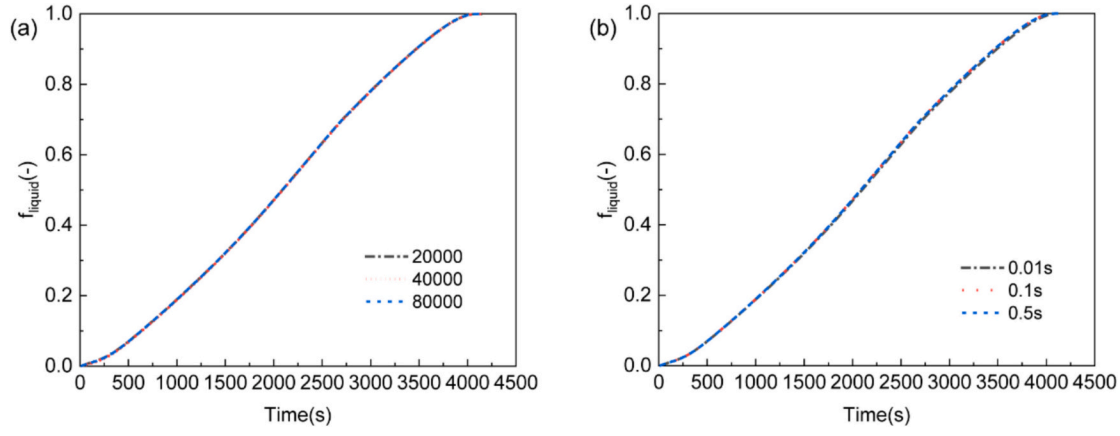

Fig. 3. Model independence analysis, (a) Grid independence and (b) Time step independence.

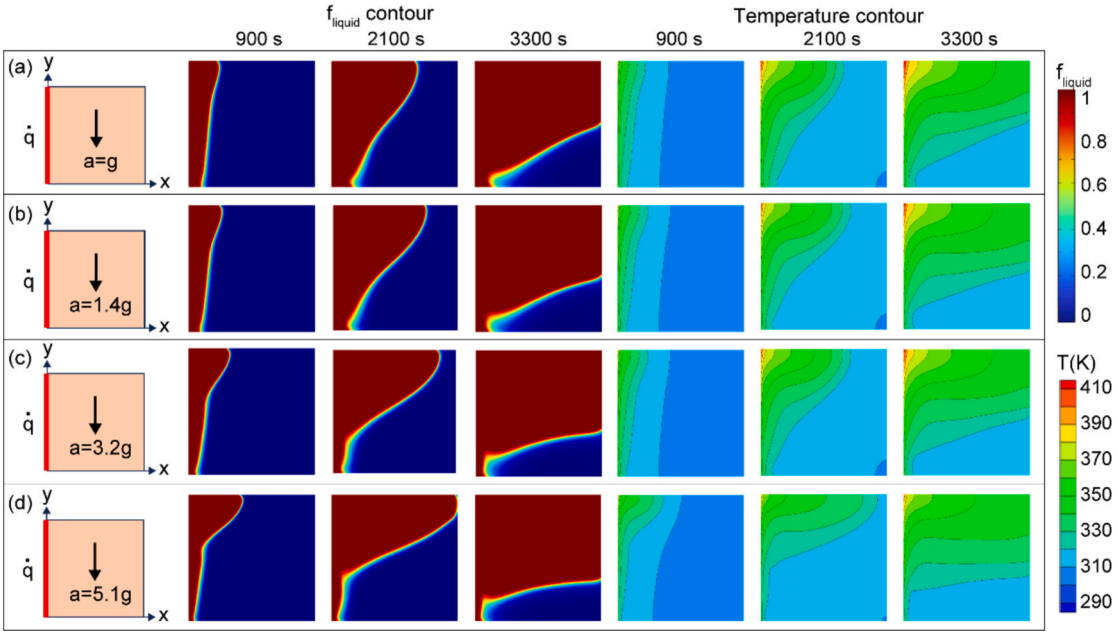

Fig. 4. Effect of supergravity on phase change characteristics of CPCMs.

distribution of PCM is uniform with a mild tilt angle appeared to the solid-liquid phase interface. The continuous phase change heat transfer facilitates the flow of liquid PCM. The transfer of thermal energy from the high-temperature fluid upwards accelerates the melting rate of the top of the container, resulting in a phase interface where the upper part melts rapidly and the lower part melts slowly. This is due to the natural convection of liquid PCM driven by the thermal buoyancy inherent to its temperature-sensitive density. More melting space and liquid PCM produce more violent natural convection. Under the large supergravity conditions (a = 3.2 g and a = 5.1 g), the top phase interface and the temperature profile exhibit a pronounced degree of bending at the initial stage, with this bending effect increasing in line with the heat transfer. This means that the transition period from thermal conduction to convection is shortened and the intensity of natural convection is enhanced in the a = 3.2 g and a = 5.1 g cases. Fig. 4 reveals that an increase in supergravity can further promote the high-temperature fluid flow, causing the more uneven temperature distribution within the container. The horizontal displacement between the top and bottom phase interfaces develops accordingly. It is noted that the PCM velocity at the solid-liquid interface decreases towards the end of the melting ($t = 300$ s). The direction of the temperature gradient tends to converge to the direction of gravity as the supergravity rises, implying that the late stage of CPCM melting mainly relies on thermal conduction, both in normal gravity and supergravity. Fig. 4 reveals that larger supergravity induces less high-temperature PCM located near the heating wall. Correspondingly, more heat is obtained and stored in the form of sensible heat in the larger supergravity case.

The phase contours and temperature profiles of CPCM under various

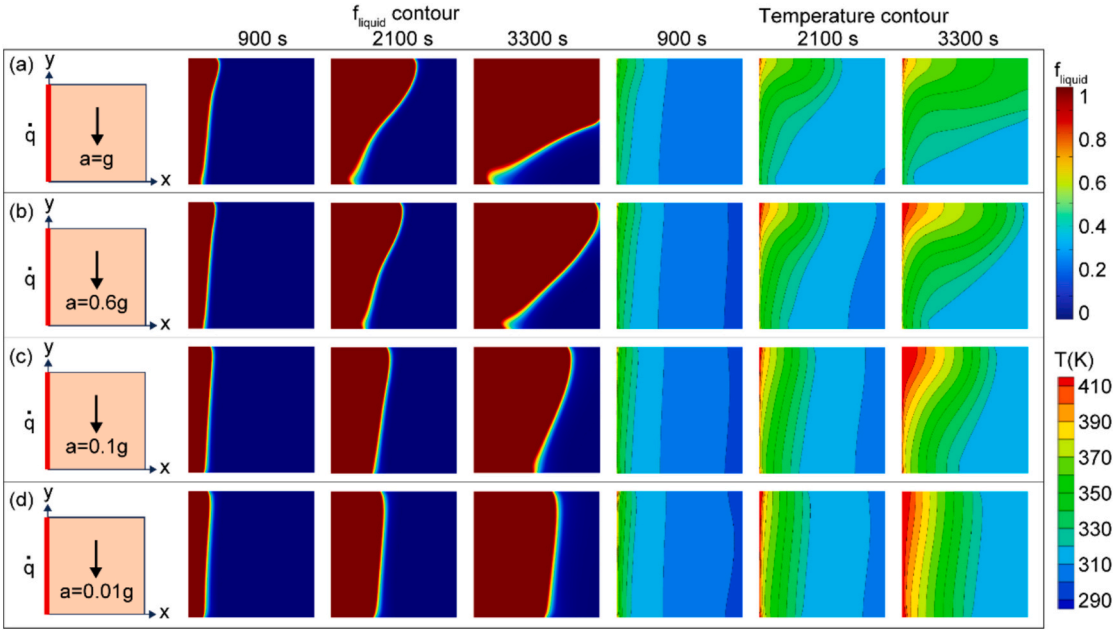

Fig. 5. Effect of microgravity on phase change characteristics of CPCMs.

microgravity conditions are illustrated in Fig. 5. Compared to the a = g case, it is found that the evolution rate of the top phase interface is slowed down and the isotherms in the temperature field are slightly curved with decline of the microgravity. This indicates that the impact of gravity on the development of natural convection is reduced and the intensity of natural convection is weakened. Particularly at a = 0.01 g, the phase interface is parallel to the heating wall surface, and the direction of the global temperature gradient is also consistent with the direction of heat flow. This means that the fluid flow can be rationally ignored under microgravity condition. The conduction is the primary heat transfer mode in the CPCM melting process. It is observed that a reduction in microgravity results in the formation of denser isotherm rows in the vicinity of the heat source within the CPCM. In summary, when the microgravity decreases, the heat transfer mechanism is characterized by a gradual weakening of convection and a gradual enhancement of conduction. Whereas, the less microgravity hardly affects the formation of the natural flow. The thermal conduction will completely dominate the phase change heat transfer, generating an inefficient CPCM melting process. PCM closer to the heating wall in microgravity cases shows higher temperature in Fig. 5, indicating that more thermal energy is stored in sensible heat. Meanwhile, the lower the microgravity, the more thermal energy is converted into sensible heat.

Fig. 6 compares the instantaneous liquid phase fraction and the average temperature of the heat wall surface under various gravity. Fig. 6(a) reports that the melting rate of PCM increases with the augment of supergravity. The flow intensity of the high-temperature fluid rises as the supergravity increases, contributing to the enhanced natural convection that is responsible for the melting process. Whereas, the supergravity is found to have limited effect on the total duration of complete melting of CPCM. The above phase interfaces and temperature profiles suggest that the flow intensity can be improved by supergravity. The phase interface develops quickly to the left side, forming a high-temperature liquid zone at the top of the container. The heat transfer between the upper liquid zone and lower solid zone is largely controlled by conduction, which leads to a deceleration of the CPCM melting rate in the latter stage. In other words, the increase of supergravity is beneficial to the convection, but has the opposite effect on the convective period, limiting its impact on the total time required for complete melting. Considering the microgravity inhibits the fluid flow, it follows that the natural convection will diminish with an increase in microgravity. Thermal conduction is unable to compensate for the loss of convection, which then contributes to longer time for complete melting under larger microgravity. Additionally, the natural convection significantly affects the heat transfer capability between the heat wall surface and CPCM. Temperature changes of the heat wall surface in Fig. 6(b) indicate that the temperature rise rate decreases with the increase of the gravity. This is attributed to the natural convection enabling to improve the heat transfer between the fluid and the heat wall surface, which in turn effectively controls the temperature rise rate at the heat wall.

Buoyancy, hydrostatic pressure, and flow instability can change under dynamic gravity, which remarkably affects the heat transfer process of CPCMs. (1) Buoyancy Force. The natural convection is driven by the buoyancy. Supergravity enlargers the buoyancy and accelerates convention heat transfer. Whereas, microgravity reduces it, leading to a conduction-dominated heat transfer. (2) Hydrostatic Pressure. Supergravity intensifies the hydrostatic pressure gradient, strengthening temperature-pressure coupling and flow instability. Conversely, microgravity eliminates it, stabilizing flow and restricting heat transfer. (3) Rayleigh Number. The natural convection can be characterized by the Rayleigh number (*Ra*). Supergravity produces large *Ra* that triggers intense natural convection within the liquid PCMs. While, microgravity generates low *Ra*, suppressing the natural convection and reducing the melting rate of CPCMs.

3.2. Pore parameter of copper foam

The above results fully confirm that supergravity enables to promote the formation of natural convection and the development of phase interfaces, whereas microgravity has opposite effect that prolongs the PCM melting time. It is identified that the pore parameters of the copper foam can affect the phase change heat transfer of CPCMs. This effect will be definitely amplified under various gravity conditions. Accordingly, this paper selects three force fields of a = 0.01 g, 1 g and 5.1 g, which correspond to microgravity, constant gravity and supergravity, with the objective of further investigating the effect of pore parameters on heat transfer of CPCM under diverse gravity conditions.

Fig. 7 analyzes the phase and temperature contours of CPCM with varying porosities at a = g. The effective copper content in the CPCM rises with a reduction in the porosity of the copper foam, noticeably enhancing the thermal conductivity of CPCM. It can be found that the lower porosity generates the larger liquid phase area and the mushy zone, as displayed at the middle stage of the phase transition (t = 2100 s). Whereas, the trends of the phase interface evolution of CPCMs are similar. Temperature contours indicate that the internal temperature gradient reduces with the decline in the copper foam porosity, forming a more uniformed CPCM temperature distribution. The phase and temperature contours associated with various pore densities show that the larger pore density induces the less phase interface offset angle, thereby creating a more parallel alignment of the isotherms. This can be attributed to two principal factors: 1) The high pore density copper foam increases the flow resistance and inhibits the natural convection development of liquid PCMs; 2) The high pore density copper foam increases the contact area between the PCM and the copper skeleton, which facilitates the development of thermal conduction along the direction of

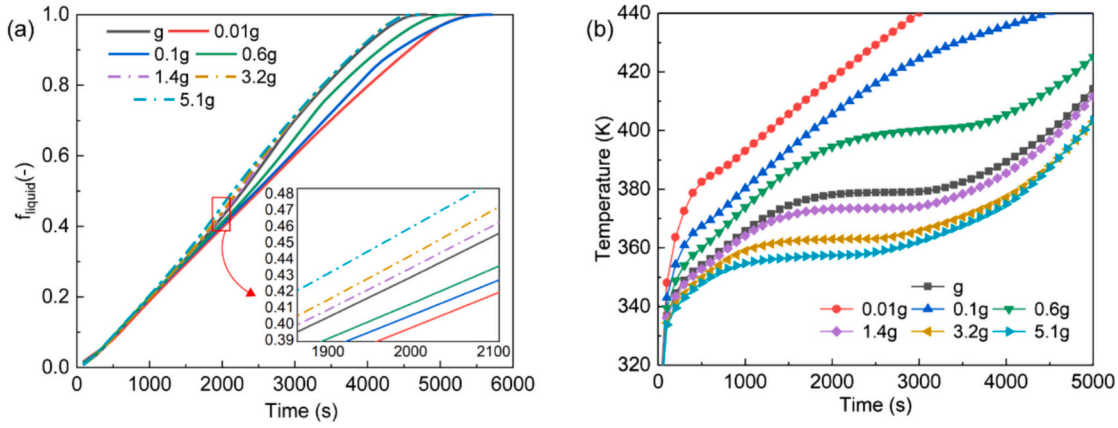

Fig. 6. Effect of gravity on liquid fraction and heat source temperature.

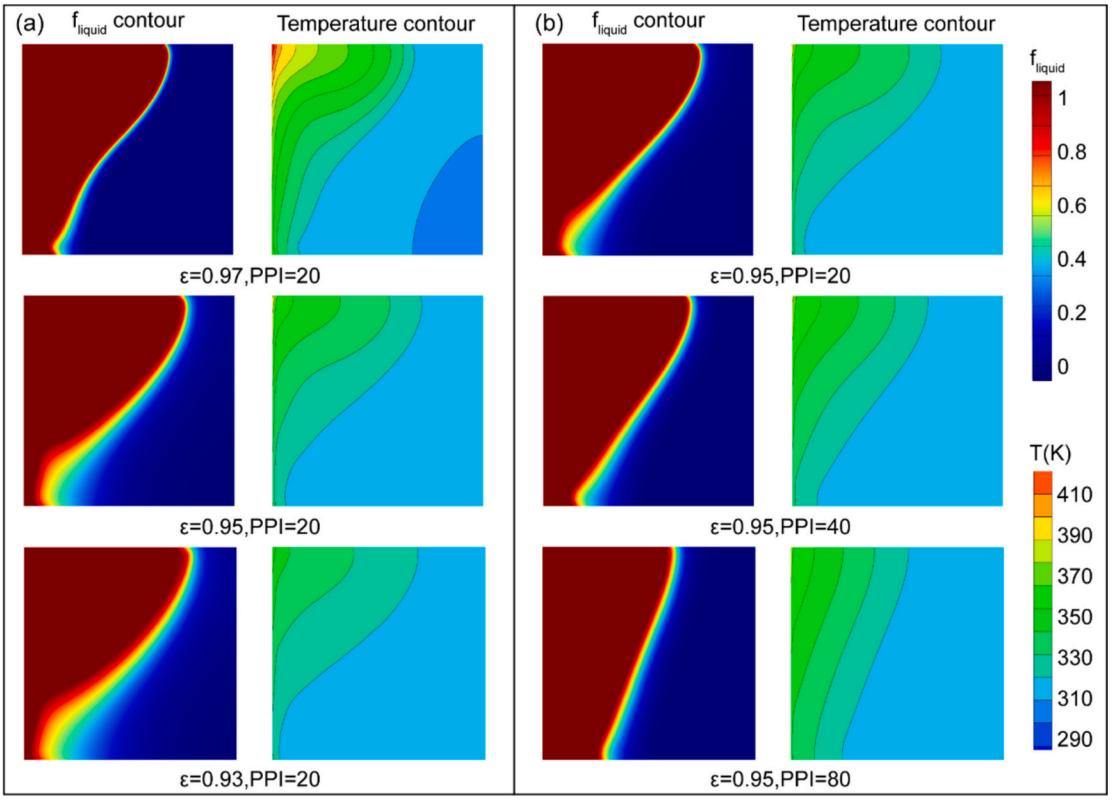

Fig. 7. Effect of the pore parameter on heat transfer of CPCM under constant gravity (t = 2100 s).

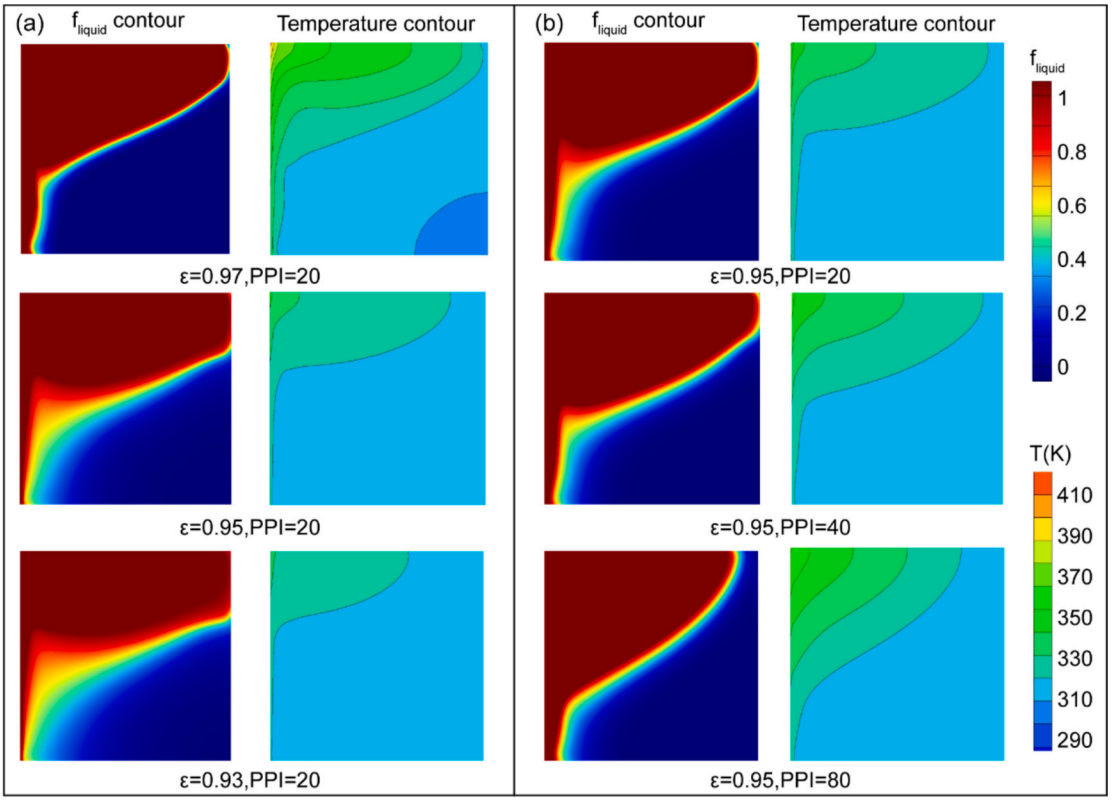

Fig. 8. Effect of the pore parameter on heat transfer of CPCM under supergravity (t = 2100 s).

heat flow. It is detected that the pore density of the copper foam exerts a more pronounced influence on the natural convection of liquid PCMs than its porosity. Supergravity of a = 5.1 g arises a highlighted thermal buoyancy that facilitates the liquid PCM to overcome the resistance posed by the copper foam skeleton.

Fig. 8 indicates that the evolution rate of the phase interface at the top of the container is markedly faster than that observed in the constant gravity case for all pore parameters. As the porosity of the copper foam increases, a non-uniform temperature distribution occurs in the mushy zone under supergravity, driven by the coupling effect of thermal conduction and convection. Whereas, the high density of the copper foam is capable of improving this temperature uneven distribution. In addition, since the natural convection in the liquid phase region under microgravity condition (a = 0.01 g) is almost entirely suppressed, thermal conduction is responsible of the PCM melting process. The phase interface evolves in parallel with the thermal wall surface for all CPCMs, as plotted in Fig. 9.

The liquid fractions of CPCMs with various pore density and porosity over time under supergravity (a = 5.1 g), normal gravity (a = g) and microgravity (a = 0.01 g) conditions are separately evaluated, in order to reveal the influence of pore parameters on the melting process. Obtained results in Fig. 10 indicate that the lower porosity causes the smaller liquid fraction of CPCMs in the pre-melting period ($t < 1300$ s). This is attributed to the fact that low porosity CPCMs have high thermal conductivity, quickly transferring thermal energy to the interior of the container. The advantage of high thermal conductivity of CPCMs with the low porosity copper foam is increasingly evident during in the middle and late melting periods. It can be inferred that the lower the porosity, the faster the melting rate and the shorter the time required to complete the melting. These results suggest that lowering the porosity of the copper foam facilitates a shorter total melting time for CPCMs and enhanced the phase transition. It is specific that the total melting time is determined as 3600 s, 3620 s and 3840 s for CPCMs with porosity of 0.97 under supergravity, normal gravity and microgravity conditions, respectively. In comparison to CPCMs with the copper foam porosity of 0.93, the corresponding total melting time is reduced by 22.1 %, 25.8 % and 30.1 %. Meanwhile, the above results indicate that high thermal conduction of CPCMs with low porosity can be fully utilized in the weak the natural convection case.

Fig. 11 illustrates the liquid fraction of CPCMs with various pore density over time. The pore density of the copper foam has lower effect on the melting rate of CPCMs in contrast to its porosity. This results from the pore density characteristics of the CPCMs. Actually, the high pore density not only enhances thermal conduction between the copper foam skeleton and the PCM, but also inhibits the development of convection. The complete melting time of CPCMs containing the copper foam with the pore density of 20 PPI, 40 PPI and 80 PPI is calculated as 4060 s, 4120 s and 4300 s under normal gravity condition (a = g).

Compared to CPCMs with the 20 PPI copper foam, the melting time increases merely by 1.5 % and 5.9 % for CPCMs with the 40 PPI and 80 PPI copper foam, respectively. However, the pore density of the copper foam enables to alter the coupling effect between thermal conduction enhancement and convective inhibition under various gravity conditions. Under the supergravity condition (a = 5.1 g), the total melting time of the CPCMs containing the copper foams with the pore density of 20 PPI, 40 PPI and 80 PPI is respectively 3980 s, 3980 s and 4020 s, implying that limited effect can be brought from the pore density of the copper foam. This can be largely explained by the fact that the buoyancy force drives the high-temperature fluid to overcome the flow resistance. The positive gain of thermal conduction caused by increasing the pore density of the copper foam is offset by the negative loss of convection, demonstrating nearly no impact on the total melting time of the CPCMs. Microgravity (a = 0.01 g) substantially suppresses natural convection of the liquid PCM. The high pore density of the copper foam produces larger contact area which facilitates the CPCM melting during the thermal conduction-driven period. Therefore, it can be established that the total melting time decreases with augment of the pore density. The total melting time of CPCM containing the copper foam with pore

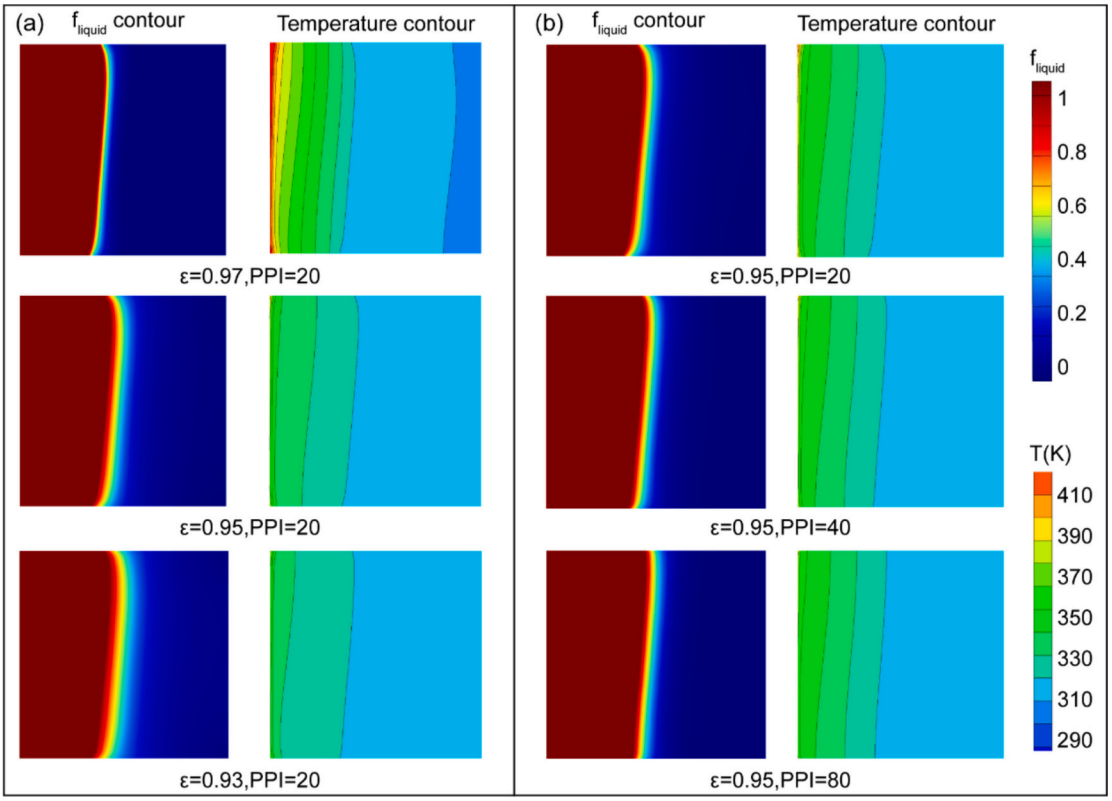

Fig. 9. Effect of the pore parameter on heat transfer of CPCM under microgravity (t = 2100 s).

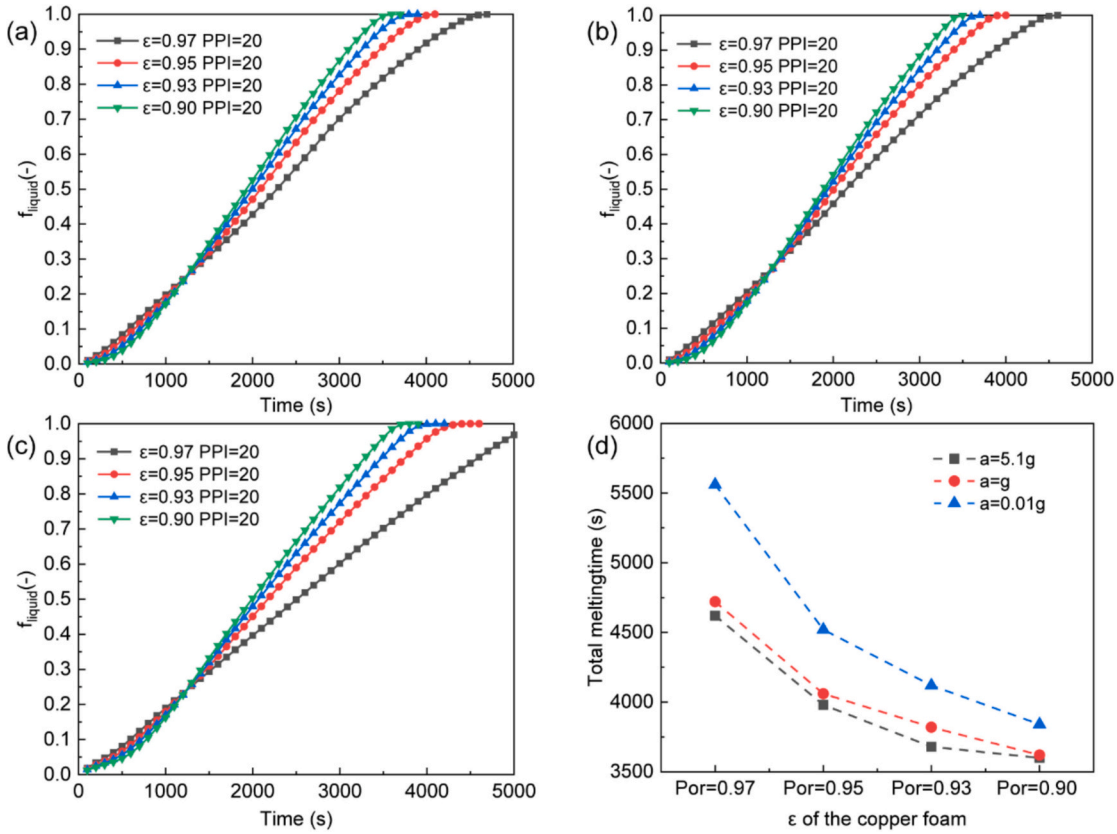

Fig. 10. Liquid fraction and total melting time of phase change units with various porosity, (a) f_{liquid} at a = g; (b) f_{liquid} at a = 5.1 g; (c) f_{liquid} at a = 0.01 g and (d) Total melting time.

density of 40 PPI and 80 PPI is 4360 s and 4240 s, representing a reduction of 3.5 % and 6.1 % compared to the case with the pore density of 20 PPI.

Fig. 12 depicts the temperature profiles of the heat wall surface as a function of the porosity of the copper foam under various gravity conditions. It can be found that temperature profiles of the heat wall surface exhibit three distinct stages when subjected to constant (a = g) and supergravity (a = 5.1 g) conditions. Specifically, the temperature of the heat wall surface rises at the initial stage of melting. It remains relatively stable during the mid-stage melting period, before resuming an upward trend at the late stage of melting. The thermal energy accumulates at the heat wall surface as a consequence of the CPCM existing as solid at the initial stage, which then evaluates the temperature of the heat wall surface. The development of natural convection at the middle stage improves the heat transfer between the heat wall surface and the CPCMs. The temperature rise rate of the heat source can be effectively controlled. The late stage of melting witnesses the slowdown of the CPCM melting rate. The CPCM absorbs heat in the form of sensible heat, presenting a challenge in controlling the temperature of the heat source. It is detected that the temperature of the heat source increases sharply over time. Microgravity (a = 0.01 g) explicitly suppresses the natural convection of liquid, resulting in the thermal energy transferred in the form of conduction. The temperature of the heat source rises linearly with elapse of time. The heat source temperature reduces as the porosity of the copper foam decreases during the melting process for all heating conditions. The CPCMs containing copper foam with lower porosity means higher effective thermal conductivity, reaching approximately 11.4 W/(m·K) for the copper foam porosity case of 0.90. The improved thermal conductivity can enhance heat transfer and eliminate the heat aggregation at the heat source. Therefore, reducing the porosity of the copper foam is beneficial to control the temperature rise rate of the heat source, and thereby improve the temperature control performance of CPCMs.

Effects of the pore density on the heat wall surface temperature under various gravity conditions are plotted in Fig. 12. The constant gravity induces the initial heat wall surface temperature decreases with increase of the pore density, which is attributed to the limited heat transfer dominated by thermal conduction. Considering the convection is restricted at the early stage of melting, the higher pore density of the copper foam means the stronger thermal conduction of the CPCMs, arising the relatively low heat wall surface temperature. Meanwhile, increasing the pore density of the copper foam is negative to the intensity of natural convection. Compared to the pore density of 20 PPI, the smooth period of the heat wall surface temperature is more hysteretic than that observed in the case of 40 PPI pore density. The copper foam with the pore density of 80 PPI greatly restricts the fluid flow and the development of natural convection. Thermal energy is transferred to the interior of the container through thermal conduction. The temperature of the heat source is increased linearly similar to the microgravity condition (a = 0.01 g). Contrarily, the supergravity condition (a = 5.1 g) promotes the migration of high-temperature fluid by means of the buoyancy force. The smooth period of the heat wall surface lags with increase of the pore density of the copper foam. Subsequently, the temperature rise rate of the heat wall becomes nearly synchronous over time. The above results indicate that CPCM with a high pore density of the copper foam is suitable for short-term temperature control. The natural convection significantly affects the temperature trend of the heat wall surface. The CPCM porosity under strong convection (a = 5.1 g) has negligible effect on the temperature control of the heat wall surface over a long period of time, whereas the low pore density structure is more conducive to the long-term temperature control under weak convection (a = g). Unlike the a = g and a = 5.1 g cases, the a = 0.01 g case leads to the lower temperature of the heat wall surface under the higher pore density, which implies that the high pore density case is suitable for full

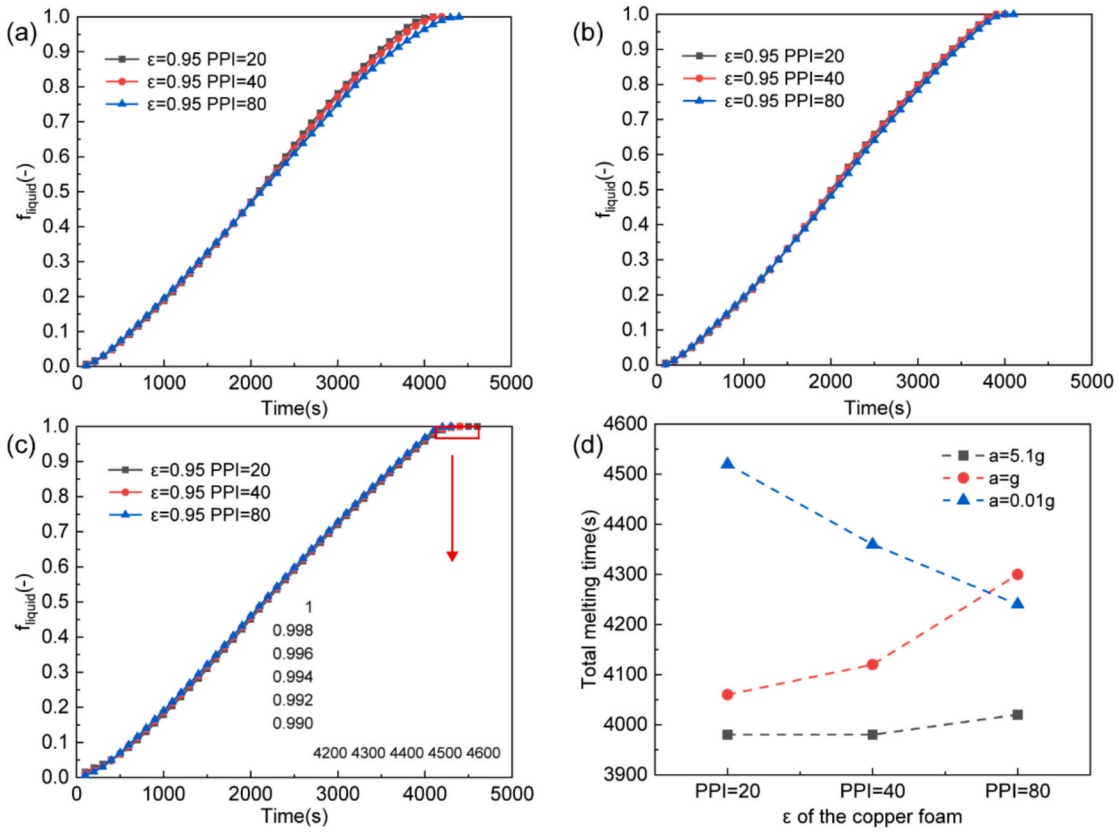

Fig. 11. Liquid fraction and total melting time of phase change units with various pore density, (a) f_{liquid} at a = g; (b) f_{liquid} at a = 5.1 g; (c) f_{liquid} at a = 0.01 g and (d) Total melting time.

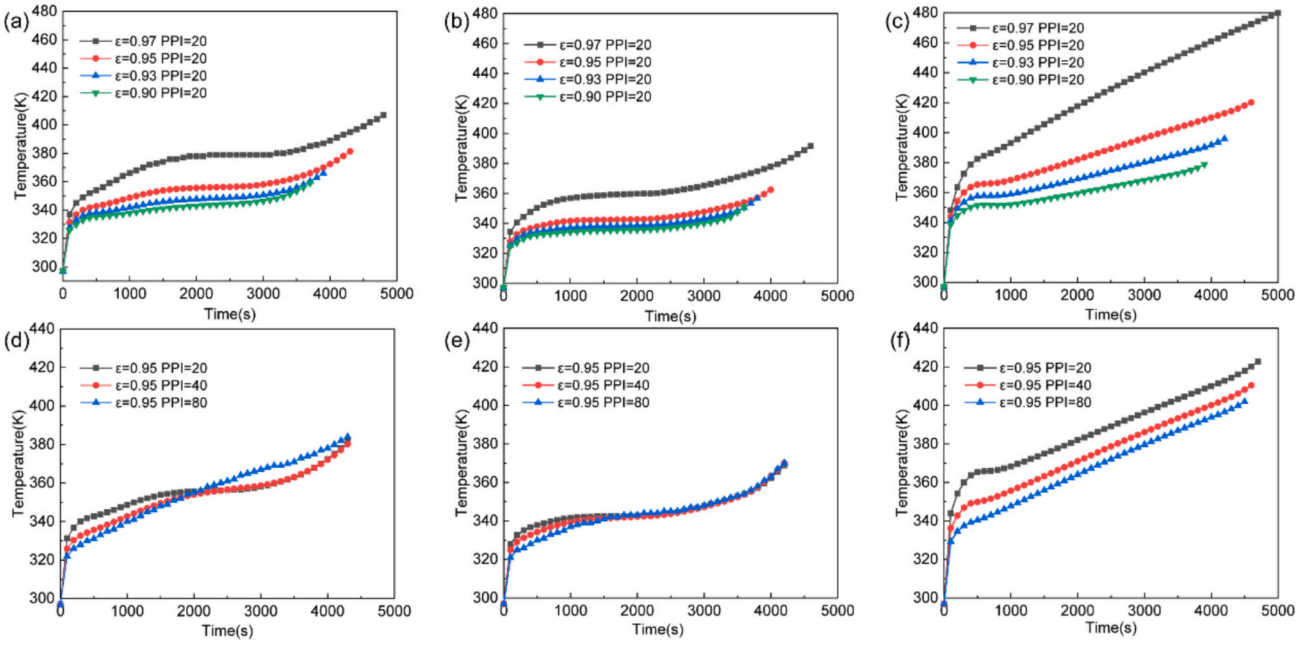

Fig. 12. Heat wall temperature of phase change units, (a) a = g, PPI = 20; (b) a = 5.1 g, PPI = 20; (c) a = 0.01 g, PPI = 20; (d) a = g, ε = 0.95; (e) a = 5.1 g, ε = 0.95 and (f) a = 0.01 g, ε = 0.95.

lifecycle temperature control of devices under microgravity. This is due to the fact that heat transferred from the heat source mainly relies on the conduction when the natural convection is completely suppressed. The higher pore density yields the denser arrangement of the pore units. The contact area between the copper foam and the PCM can be improved, which facilitates the heat conducted from the heat source to the CPCM.

3.3. Gradient non-uniform enhancement

Since heat transfer performance of the CPCM can be noticeably affected by the pore characteristics of the copper foam, a strategy of non-uniform arrangement of the copper foam is then designed. The total mass of the copper foam incorporated in the CPCM is constant under the average porosity of 0.95. A low-porosity copper foam ($\varepsilon = 0.93$) is placed in the solid shrinking region. Whereas, a high-porosity copper foam ($\varepsilon = 0.97$) is placed in the liquid convection region. It is expected that the structure optimization strategy aims to regulate the interaction between thermal conduction and convection during the phase change process to achieve enhanced thermal storage performance. The structures of four non-uniform gradient copper foams (Case-1–4) are established in Fig. 13.

Fig. 14 and Fig. 15 show the transient phase interface contours of the four gradient non-uniform phase change units. The high porosity copper foam is placed near the heat wall surface in the Case-1. This leads to significant natural convection at the initial and middle melting stages. The heat is rapidly aggregated at the top of the container as the melting proceeds. The low-porosity copper foam stays away from the heat wall surface. The enhanced thermal conduction results in the hot fluid gathered at the top of the container. Heat is transferred from the right top to the left bottom region, which in turn forms solid shrinkage regions at the left bottom of the container. The top high-temperature fluid layer forms earlier and the bottom-up thermal conduction becomes more significant under supergravity gravity.

Compared to the normal gravity, the melting rate of CPCM under supergravity condition at the rear exceeds that at the front. The fluid under the gradient structure of the copper foam needs to traverse the non-uniform pores from the low porosity region to the high porosity region, impeding the flow development of the liquid PCM. Both Case-2 and Case-3 structures reduce the average porosity of the copper foam at the bottom of the containers, which then improves the thermal conduction along the horizontal direction and the area of the mushy zone. The lower-porosity copper foam existed close to the heat wall surface in Case-4 restricts the fluid mobility. Consequently, development of the natural convection during the CPCM melting is limited, resulting in a reduced PCM migration rate at the top phase interface. Meanwhile, the less porosity corresponds to the larger thermal conductivity. The melting rate of the CPCM along the bottom diagonal direction is increased. The shrinkage rate of the solid in this area lags significantly behind those of other gradient structures at the late stage.

Fig. 16 displays heat storage performance of phase change units in terms of liquid fraction, heat storage rate and total melting time. The melting process of CPCM is analogous to that observed at normal gravity and supergravity conditions. Various structures of the phase change units mainly affect the melting rate of CPCM at the middle and late stages. Case-2 presents that the high porosity area at the left top of the container is largest, which favors the development of liquid natural convection at the early stage. As the melting proceeds, the low porosity area at the bottom of the container rises, while the expansion of the overall liquid layer thickness suppresses the contribution of natural convection to the CPCM melting. The related melting rate of CPCM embedded in Case-2 declines at the middle stage. The fluid needs to flow from the low porosity area to the high porosity areas at the early melting stage in Case-3, inhibiting the development of liquid natural convection. The CPCM melting rate lags significantly compared to the uniform phase change units. The low-porosity copper foam arranged in the bottom of Case-3 implies that the thermal convection is weakened as the phase transition progresses. The CPCM has a higher longitudinal thermal conduction advantage at the later stage. The liquid fraction of CPCM in

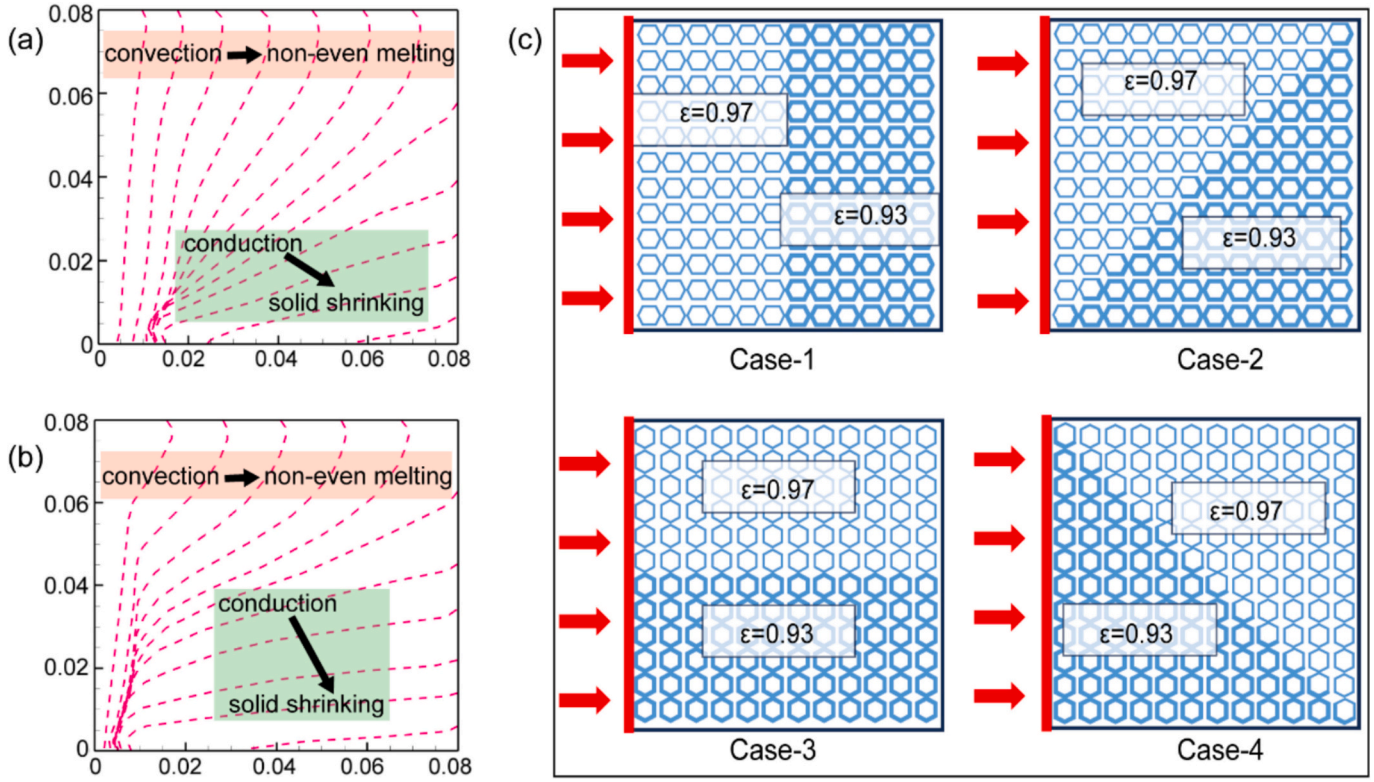

Fig. 13. Schematics of phase change units containing gradient copper foams, (a) Phase change heat transfer of CPCMs ($\varepsilon = 0.95$, a = g); (b) Phase change heat transfer of CPCMs ($\varepsilon = 0.95$, a = 5.1 g) and (c) schematics of gradient copper foams (ε).

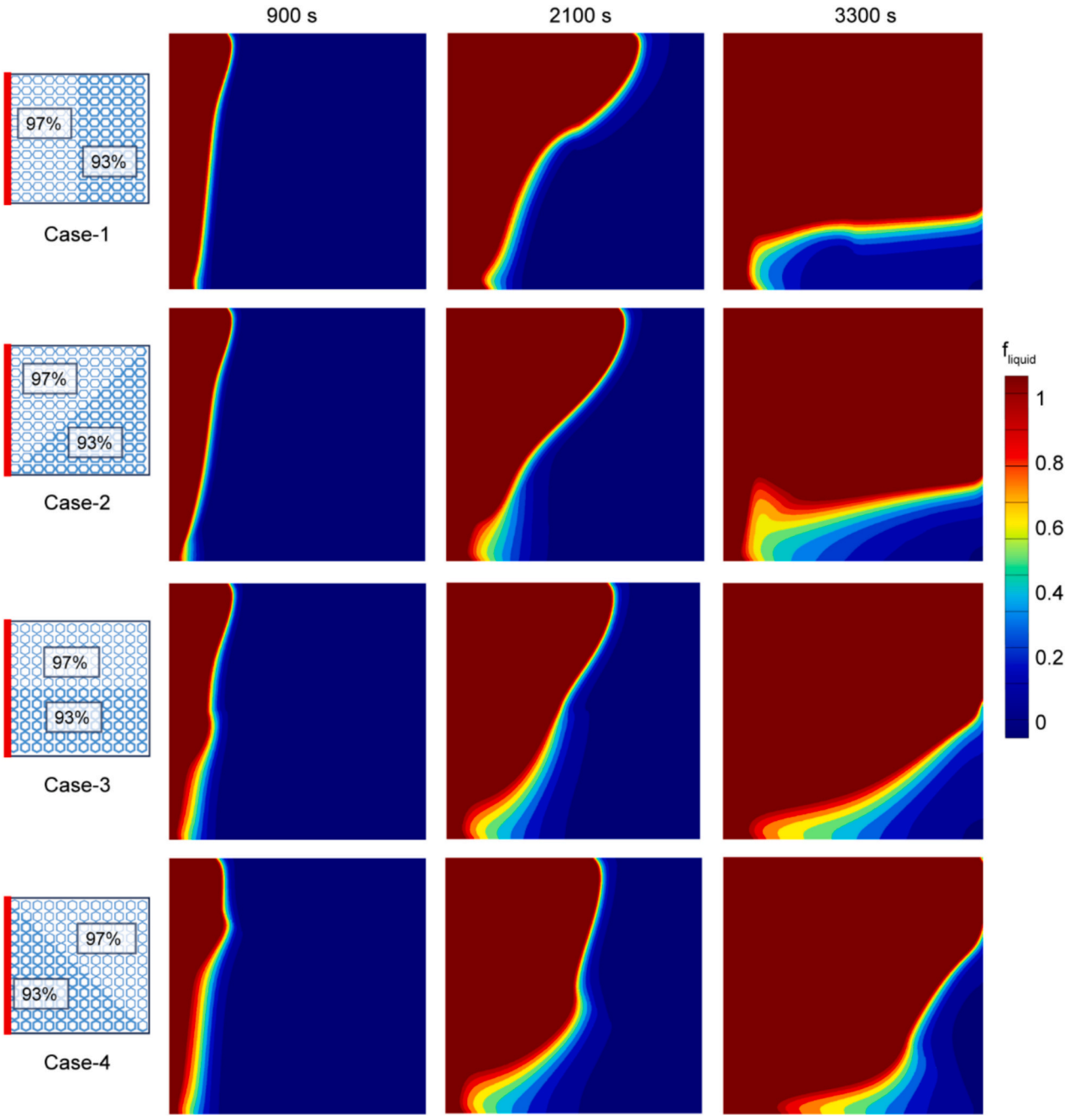

Fig. 14. Transient phase contours of gradient CPCMs under constant gravity (a = g).

Case-3 exceeds that of the uniform structure at 3100 s and 2750 s under normal gravity and supergravity conditions, respectively.

In contrast, the high thermal conduction of the low porosity structure in the left diagonal region of Case-4 can compensate for the loss of convection at the early stage. The melting rate of CPCM is comparable to that of the uniform structure. Whereas, the high-porosity copper foam placed in the back-end of the structure is detrimental to the conduction-dominated CPCM melting process at the later stage. CPCM in Case-1 and Case-4 forms a solid shrinkage region that is difficult to melt, thus prolonging the melting period. The low porosity copper foam (Case-2 and Case-3) arranged in the right bottom region facilitates the melting process, achieving reduction in the total melting time. The strengthening effect to the CPCM melting process is most obvious in the Case-3 both under normal gravity and supergravity conditions. Compared to the uniform structure, the total time to completely melt CPCM is reduced by 6.2 % with the latent heat storage rate increased by 6.5 % in the normal gravity case. Similarly, the total melting time of CPCM is reduced by 6.7 % with an increase of 7 % in the latent heat storage rate in the supergravity case.

4. Conclusions

This paper investigates the effects of various pore parameters of the copper foam on heat transfer performance of PCM under microgravity and supergravity conditions. The related volumetric forces are achieved by equivalent static forces combined with gravity and centrifugal acceleration. The direction of the heat flow is consistently maintained perpendicular to that of the combined working force during the investigation. A local strengthening strategy of copper foam gradient layout is proposed to address the non-uniform melting behavior of CPCM. The

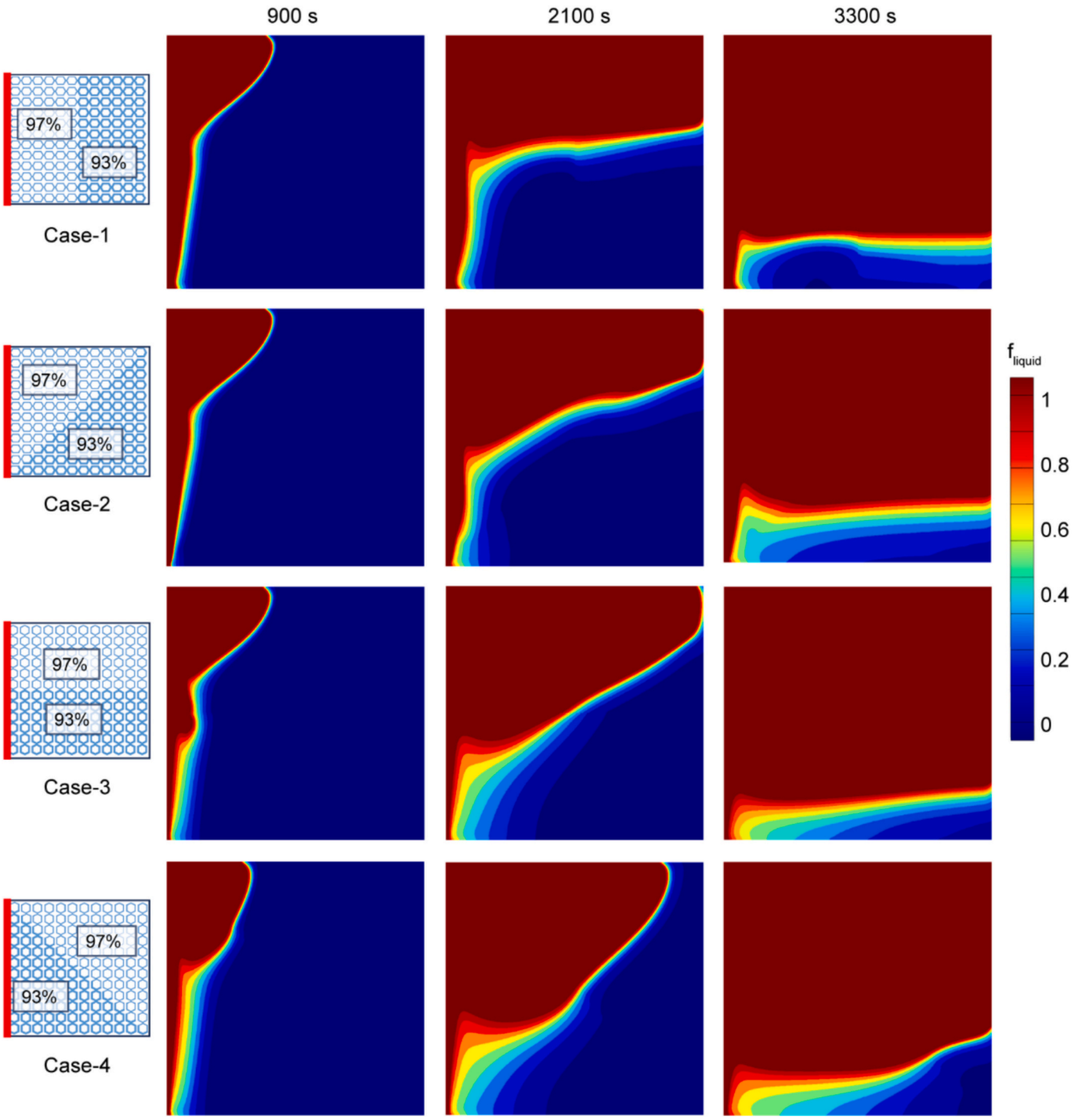

Fig. 15. Transient phase contours of gradient CPCMs under supergravity (a = 5.1 g).

main conclusions can be drawn as follows:

(1) The supergravity noticeably affects the natural convection of liquid that is positive to evolution of the phase interface. The microgravity significantly inhibits the flow of liquid, leading to a slower melting rate of CPCM in comparison to other cases.
(2) The natural convection of liquid increases with the augment of gravity. No obvious changes in the total melting time of CPCM ($\varepsilon = 0.93$) can be found under supergravity and microgravity conditions. The heat wall surface temperatures are reduced by 7 K and 49 K compared to normal gravity cases.
(3) The pore density of copper foam substantially affects the evolution of the phase interface under supergravity condition. The melting time of CPCM containing the copper foam with pore density of 80 PPI is shortened by 6.1 %, with the heat wall surface temperature 21 K lower than the pore density case of 20 PPI.
(4) The high-porosity in upper and the low-porosity in bottom structure has excellent melting rate and heat storage performance over the uniform phase change unit. The total melting time of supergravity case is shortened by 6.7 %, with the heat storage rate enhanced by 7.0 %.
(5) The gradient structure optimization scheme provides a simple and cost-effective strategy to improve the no-uniform melting

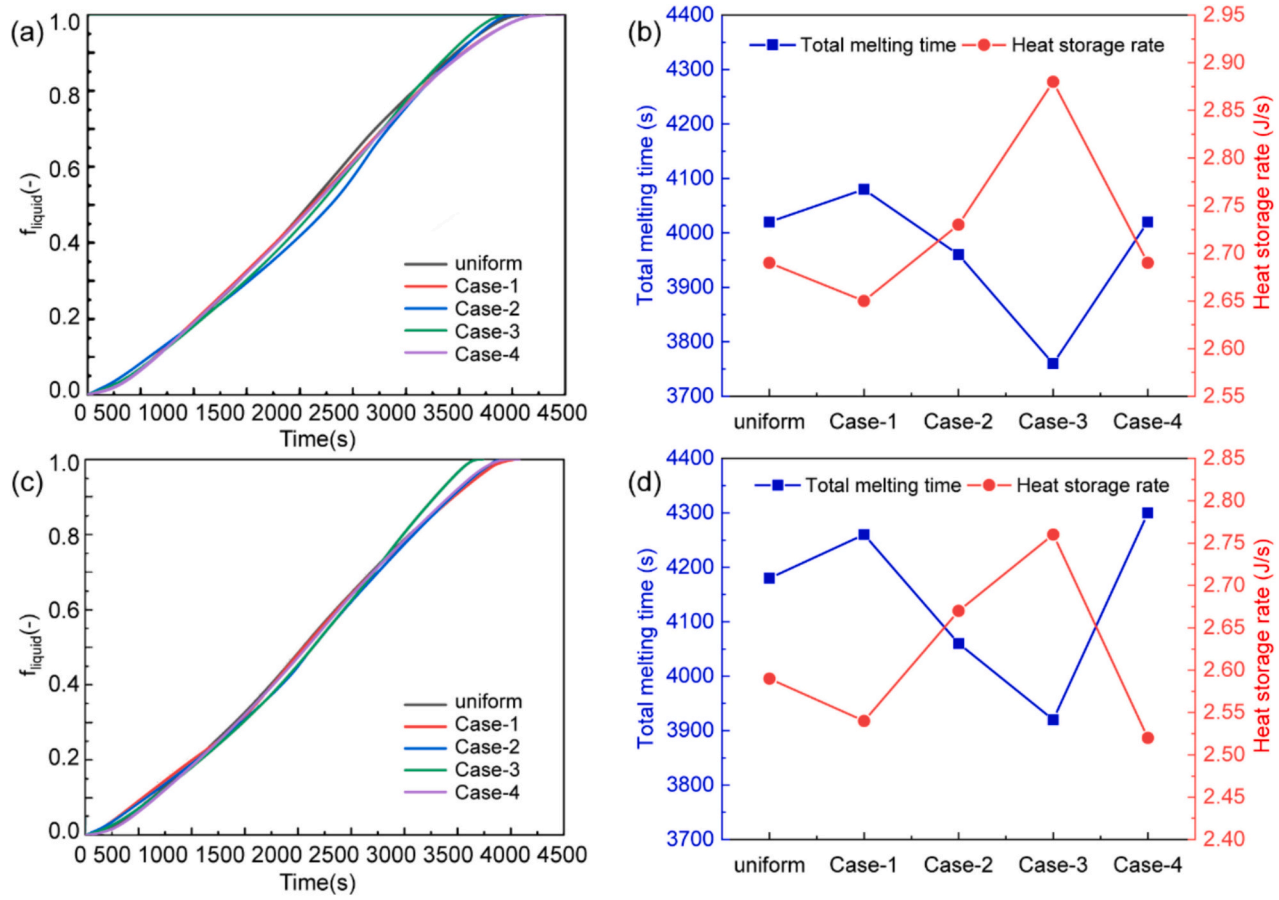

Fig. 16. Heat storage performance of phase change units, (a) f_{liquid} at a = g, (b) Melting time and heat storage rate at a = g, (c) f_{liquid} at a = 5.1 g and (d) Melting time and heat storage rate at a = 5.1 g.

issue of CPCMs. The CPCMs with enhanced thermal performance could benefit the thermal management of high-power electronics applied in aerospace, power and shipping fields.

CRediT authorship contribution statement

Zhaoli Zhang: Writing – original draft, Validation, Supervision, Funding acquisition. **Guoqin Wang:** Methodology, Investigation, Data curation. **Nan Zhang:** Writing – review & editing, Validation, Formal analysis. **Daniela Dzhonova:** Writing – review & editing, Supervision, Resources. **Shady Attia:** Writing – review & editing, Supervision, Methodology. **Yanping Yuan:** Writing – review & editing, Validation, Methodology.

Declaration of competing interest

The authors declare that they have no known competing financial interests or personal relationships that could have appeared to influence the work reported in this paper.

Acknowledgments

The work is supported by the National Natural Science Foundation of China (No: 52108077 and 52311530700) and Fundamental Research Funds for the Central Universities (No.: 2682024CX104 and 2682024GF021).

Data availability

Data will be made available on request.

References

[1] Z. He, Y. Yan, Z. Zhang, Thermal management and temperature uniformity enhancement of electronic devices by micro heat sinks: a review, Energy 216 (2021) 119223, https://doi.org/10.1016/j.energy.2020.119223.
[2] J. Mathew, S. Krishnan, A review on transient thermal management of electronic devices, J. Electron. Packag. 144 (2021) 010801, https://doi.org/10.1115/1.4050002.
[3] R.A. Lawag, H.M. Ali, Phase change materials for thermal management and energy storage: a review, J. Energy Storage 55 (2022) 105602, https://doi.org/10.1016/j.est.2022.105602.
[4] A.L. Moore, L. Shi, Emerging challenges and materials for thermal management of electronics, Mater. Today 17 (2014) 163–174, https://doi.org/10.1016/j.mattod.2014.04.003.
[5] L. Song, Y. Zheng, Z. Xiao, C. Wang, T. Long, Review on thermal runaway of lithium-ion batteries for electric vehicles, J. Electron. Mater. 51 (2022) 30–46, https://doi.org/10.1007/s11664-021-09281-0.
[6] X. Feng, M. Ouyang, X. Liu, L. Lu, Y. Xia, X. He, Thermal runaway mechanism of lithium ion battery for electric vehicles: a review, Energy Storage Mater. 10 (2018) 246–267, https://doi.org/10.1016/j.ensm.2017.05.013.
[7] M. Zhi, R. Fan, X. Yang, L. Zheng, S. Yue, Q. Liu, Y. He, Recent research progress on phase change materials for thermal management of lithium-ion batteries, J. Energy Storage 45 (2022) 103694, https://doi.org/10.1016/j.est.2021.103694.
[8] F. Agyenim, N. Hewitt, P. Eames, M. Smyth, A review of materials, heat transfer and phase change problem formulation for latent heat thermal energy storage systems (LHTESS), Renew. Sustain. Energy Rev. 14 (2010) 615–628, https://doi.org/10.1016/j.rser.2009.10.015.
[9] K.S. Reddy, V. Mudgal, T.K. Mallick, Review of latent heat thermal energy storage for improved material stability and effective load management, J. Energy Storage 15 (2018) 205–227, https://doi.org/10.1016/j.est.2017.11.005.
[10] M. Ghalambaz, S.A.M. Mehryan, S.R. Ramezani, A. Hajjar, M. El Kadri, M.S. Islam, O. Younis, M. Ghodrat, Phase change heat transfer in a vertical metal foam-phase change material thermal energy storage heat dissipator, J. Energy Storage 66 (2023) 107370, https://doi.org/10.1016/j.est.2023.107370.
[11] C. Xu, H. Zhang, G. Fang, Review on thermal conductivity improvement of phase change materials with enhanced additives for thermal energy storage, J. Energy Storage 51 (2022) 104568, https://doi.org/10.1016/j.est.2022.104568.

[12] A. Parida, A. Bhattacharya, P. Rath, Effect of convection on melting characteristics of phase change material-metal foam composite thermal energy storage system, J. Energy Storage 32 (2020) 101804, https://doi.org/10.1016/j.est.2020.101804.
[13] S. Wu, T. Yan, Z. Kuai, W. Pan, Thermal conductivity enhancement on phase change materials for thermal energy storage: a review, Energy Storage Mater. 25 (2020) 251–295, https://doi.org/10.1016/j.ensm.2019.10.010.
[14] A.K. S.r., S. Suresh, M. V.C., P. Kalidoss, J.S. M, D. S., P.S. Gavaskar, Experimental and numerical investigation on the performance of binary solid-solid phase change materials with integrated heat pipe and aluminium foam based heat sink for thermal management of electronic systems, Int. J. Therm. Sci. 208 (2025) 109409, https://doi.org/10.1016/j.ijthermalsci.2024.109409.
[15] M. Iasiello, M. Mameli, S. Filippeschi, N. Bianco, Metal foam/PCM melting evolution analysis: orientation and morphology effects, Appl. Therm. Eng. 187 (2021) 116572, https://doi.org/10.1016/j.applthermaleng.2021.116572.
[16] X.K. Yu, Y.B. Tao, Y. He, Z.C. Lv, Temperature control performance of high thermal conductivity metal foam/paraffin composite phase change material: an experimental study, J. Energy Storage 46 (2022) 103930, https://doi.org/10.1016/j.est.2021.103930.
[17] F. Alimi, H.S.S. Aljibori, M. Bouzidi, A. Alasmari, S. Yazdani, M. Ghalambaz, Enhancing LHTES efficiency using asymmetric hexagon anisotropic metal foam layer: a comparative study on orientation and scale, J. Build. Eng. 98 (2024) 111040, https://doi.org/10.1016/j.jobe.2024.111040.
[18] W.-C. Feng, B. Ding, Y. Zhang, M.-F. Mu, L. Gong, How can copper foam better promote the melting process of phase change materials, Int. J. Therm. Sci. 187 (2023) 108199, https://doi.org/10.1016/j.ijthermalsci.2023.108199.
[19] G. Shu, T. Xiao, J. Guo, P. Wei, X. Yang, Y.-L. He, Effect of charging/discharging temperatures upon melting and solidification of PCM-metal foam composite in a heat storage tube, Int. J. Heat Mass Transf. 201 (2023) 123555, https://doi.org/10.1016/j.ijheatmasstransfer.2022.123555.
[20] Z. Zhang, J. Liu, N. Zhang, X. Cao, Y. Yuan, M. Sultan, S. Attia, Coupling effect of radiative cooling and phase change material on building wall thermal performance, J. Build. Eng. 82 (2024) 108344, https://doi.org/10.1016/j.jobe.2023.108344.
[21] W.Q. Li, T.Y. Zhang, B.B. Li, Z.R. Xue, H. Wang, D. Zhang, Enhanced energy management performances of passive cooling, heat storage and thermoelectric generator by using phase change material saturated in metal foam, Int. J. Therm. Sci. 184 (2023) 107869, https://doi.org/10.1016/j.ijthermalsci.2022.107869.
[22] Z. Wang, J. Gui, L. Zhu, H. Zhang, B. Dou, G. Yu, M. Song, L. Jiang, X. Xiao, The effect of heat flux on enhancement heat transfer mechanism in copper metal foam composite paraffin wax during melting process: experimental and simulation research, Int. J. Heat Mass Transf. 226 (2024) 125523, https://doi.org/10.1016/j.ijheatmasstransfer.2024.125523.
[23] A. Alasmari, H.S.S. Aljibori, F. Alimi, M. Bouzidi, M.S. Islam, S. Yazdani, M. Ghalambaz, A shell-tube latent heat thermal energy storage: influence of metal foam inserts in both shell and tube sides, Int. Commun. Heat Mass Transf. 159 (2024) 107992, https://doi.org/10.1016/j.icheatmasstransfer.2024.107992.
[24] X. Yang, Q. Bai, Z. Guo, Z. Niu, C. Yang, L. Jin, T.J. Lu, J. Yan, Comparison of direct numerical simulation with volume-averaged method on composite phase change materials for thermal energy storage, Appl. Energy 229 (2018) 700–714, https://doi.org/10.1016/j.apenergy.2018.08.012.
[25] A. Diani, M. Campanale, Transient melting of paraffin waxes embedded in aluminum foams: experimental results and modeling, Int. J. Therm. Sci. 144 (2019) 119–128, https://doi.org/10.1016/j.ijthermalsci.2019.06.004.
[26] X. Meng, L. Yan, J. Xu, F. He, H. Yu, M. Zhang, Effect of porosity and pore density of copper foam on thermal performance of the paraffin-copper foam composite phase-change material, Case Stud. Therm. Eng. 22 (2020) 100742, https://doi.org/10.1016/j.csite.2020.100742.
[27] M. Mozaffari, A. Hajjar, M. Sheremet, O. Younis, M. Ghalambaz, Enhancing LHTES efficiency using asymmetric hexagon anisotropic metal foam layer: a comparative study on orientation and scale, Therm. Sci. Eng. Progress 59 (2025) 103343, https://doi.org/10.1016/j.tsep.2025.103343.
[28] V. Joshi, M.K. Rathod, Constructal enhancement of thermal transport in metal foam-PCM composite-assisted latent heat thermal energy storage system, Numer. Heat Transf. A Appl. 75 (2019) 413–433, https://doi.org/10.1080/10407782.2019.1599270.
[29] Z. Shen, J. Hua, Y. He, F. Jiao, J. Wang, Experimental study of melting on graded metal foam composite phase change materials under nonuniform heat flux, Int. J. Heat Mass Transf. 239 (2025) 126613, https://doi.org/10.1016/j.ijheatmasstransfer.2024.126613.
[30] J. Guo, Z. Li, P. Wei, L. Li, X. Yang, Y.-L. He, K. Hooman, Optimization of adaptive metal foam arrangement in a heat storage tank, Int. J. Heat Mass Transf. 213 (2023) 124278, https://doi.org/10.1016/j.ijheatmasstransfer.2023.124278.
[31] X. Li, J. Duan, T. Simon, T. Ma, T. Cui, Q. Wang, Nonuniform metal foam design and pore-scale analysis of a tilted composite phase change material system for photovoltaics thermal management, Appl. Energy 298 (2021) 117203, https://doi.org/10.1016/j.apenergy.2021.117203.
[32] A. Kotb, S. Wang, Enhanced thermal storage performance with non-linear porosity distribution in copper foam-PCM composites, J. Energy Storage 105 (2025) 114612, https://doi.org/10.1016/j.est.2024.114612.
[33] H. Liu, N. Zhang, X. Li, Z. Tong, X. Cao, Y. Du, Y. Yuan, Numerical study on the thermal performance of foam-metal composite phase change material in different force fields, Int. J. Heat Mass Transf. 211 (2023) 124181, https://doi.org/10.1016/j.ijheatmasstransfer.2023.124181.
[34] Y. Wu, X. Zhang, X. Xu, X. Lin, L. Liu, A review on the effect of external fields on solidification, melting and heat transfer enhancement of phase change materials, J. Energy Storage 31 (2020) 101567, https://doi.org/10.1016/j.est.2020.101567.
[35] H. Liu, N. Zhang, Z. Zhang, Q. Xia, Y. Yuan, X. Cao, Experimental investigation of the effect of external forces on convection-driven melting of phase change material in a rectangular enclosure, Int. J. Heat Mass Transf. 199 (2022) 123489, https://doi.org/10.1016/j.ijheatmasstransfer.2022.123489.
[36] Z. Peng, Q. Gao, Z. Zhang, N. Zhang, Y. Du, Y. Yuan, M. Sultan, Heat transfer performance of copper foam/paraffin composite phase change material under different centrifugal forces-a visual experimental study, Int. J. Heat Mass Transf. 226 (2024) 125475, https://doi.org/10.1016/j.ijheatmasstransfer.2024.125475.
[37] C. Zhao, M. Opolot, M. Liu, F. Bruno, S. Mancin, K. Hooman, Numerical study of melting performance enhancement for PCM in an annular enclosure with internal-external fins and metal foams, Int. J. Heat Mass Transf. 150 (2020) 119348, https://doi.org/10.1016/j.ijheatmasstransfer.2020.119348.
[38] C. Nie, J. Liu, S. Deng, Effect of geometry modification on the thermal response of composite metal foam/phase change material for thermal energy storage, Int. J. Heat Mass Transf. 165 (2021) 120652, https://doi.org/10.1016/j.ijheatmasstransfer.2020.120652.
[39] X. Li, T. Ma, J. Liu, H. Zhang, Q. Wang, Pore-scale investigation of gravity effects on phase change heat transfer characteristics using lattice Boltzmann method, Appl. Energy 222 (2018) 92–103, https://doi.org/10.1016/j.apenergy.2018.03.184.
[40] K. Kansara, V.K. Singh, R. Patel, R.R. Bhavsar, A.P. Vora, Numerical investigations of phase change material (PCM) based thermal control module (TCM) under the influence of low gravity environment, Int. J. Heat Mass Transf. 167 (2021) 120811, https://doi.org/10.1016/j.ijheatmasstransfer.2020.120811.
[41] X. Li, Z. Zhu, Z. Xu, T. Ma, H. Zhang, J. Liu, X. Wang, Q. Wang, A three-dimensional pore-scale lattice Boltzmann model for investigating the supergravity effects on charging process, Appl. Energy 254 (2019) 113507, https://doi.org/10.1016/j.apenergy.2019.113507.
[42] C. Ding, C. Zhang, L. Ma, A. Sharma, Numerical investigation on melting behaviour of phase change materials/metal foam composites under hypergravity conditions, Appl. Therm. Eng. 207 (2022) 118153, https://doi.org/10.1016/j.applthermaleng.2022.118153.
[43] J. Luo, Y. Yuan, M.M. Joybari, X. Cao, Development of a prediction-based scheduling control strategy with V2B mode for PV-building-EV integrated systems, Renew. Energy 224 (2024) 120237, https://doi.org/10.1016/j.renene.2024.120237.
[44] L. Wang, A. Kan, W. Yu, Melting behavior and heat transfer performance in a modified PCM-filled enclosure with fins under hypergravity conditions, Int. Commun. Heat Mass Transf. 138 (2022) 106415, https://doi.org/10.1016/j.icheatmasstransfer.2022.106415.
[45] V.V. Calmidi, R.L. Mahajan, Forced convection in high porosity metal foams, J. Heat Transfer 122 (2000) 557–565, https://doi.org/10.1115/1.1287793.
[46] K. Boomsma, D. Poulikakos, On the effective thermal conductivity of a three-dimensionally structured fluid-saturated metal foam, Int. J. Heat Mass Transf. 44 (2001) 827–836, https://doi.org/10.1016/S0017-9310(00)00123-X.